Research Article

SOHAG JOURNAL OF SCIENCES

https://doi.org/10.21608/sjsci.2024.297013.1211

Characteristics of Matulla Reservoir in Saqqara Oil Field, Gulf of Suez, Egypt

Abdelbaset. M. Abudeif[*,1], Ahmed.E. Radwan[2], Mohammed A. Mohammed[1] and Faten A. Tawfik[1]

[1] *Geology Department, Faculty of Science, Sohag University, Sohag 82524, Egypt.*
[2] *Faculty of Geography and Geology, Institute of Geological Sciences, (Uniwersytet Jagielloński) Jagiellonian University in Krakow, Poland.*
[*]*Email: a.abudeif@science.sohag.edu.eg*

Received: 30th June 2024, **Revised:** 1st August 2024, **Accepted:** 24th August 2024
Published online: 19th September 2024

Abstract: The Late Cretaceous Matulla Formation is a major reservoir in Saqqara Oil Field in the Gulf of Suez Basin. The Matulla Formation exhibits varying reservoir qualities due to different lithologies, lateral facies fluctuations and complex reservoir architecture. These factors challenge effective reservoir development in the Gulf of Suez Basin. The primary objective of this study is to evaluate the hydrocarbon potentiality of the Matulla reservoirs in the Saqqara field, by assessing their petrophysical properties. This investigation is based on the wireline log analysis of two wells (GS323-1 and GS323-2A) drilled in the Saqqara field. Petrophysical characteristics of the Matulla sandstones according to the examination of well logging data indicate that they may serve as reservoirs in the field under study. These reservoirs exhibit moderate net pay thicknesses ranging between 25 and 150 feet, good net/gross ratios from 30 to 50%, low shale contents from 2% to 4%, good total porosity from 13% to 14%, effective porosities from 12.5% to 13.7%, good permeability from 219.4 mD to 320.7 mD, water saturation from 30% to 50%, and high hydrocarbon saturation from 55% to 65%. The efficiency of progressively utilising this reservoir along the Gulf of Suez Basin is consequently impacted by the aforementioned reservoir problems. The petrophysical model illustrates the ability of the Matulla reservoir to produce and retain oil. The middle and lower zones of the Matulla reservoir show the high-quality characters, while its upper zone has the low-quality characters.
Keywords: Formation evaluation, Reservoir characterization, Matulla Formation, Well logging, Gulf of Suez, net pay thickness, net/gross ratios, porosities, saturations.

1. Introduction

Nearly a century ago, near Ras Gemsa, oil exploration got underway in the Gulf of Suez. Nowadays, the Gulf is a well-known oil region with enormous hydrocarbon potential. About 80 oil fields spread throughout pre-Cambrian to Quaternary reservoirs make up this basin, with reserves ranging from 1350 to 1 million barrels [1]. Right now, among the world's major grabens or rift basins, it ranks as the fifth most productive.

The Gulf of Suez is situated in the northeast of the nation. It is a narrow body of water that is between 50 and 90 km wide [2]. Proven oil covers an area of around 38500 km^2. The Oligocene-Miocene saw the beginning of the tectonic structure of the Gulf of Suez, which led to rotating fault blocks and discernible sedimentary disconformities [3,4]. The major hydrocarbon discoveries in the Gulf of Suez are mostly located on this sloping fault block.

Four tectonic provinces: the northernmost, the north central, the south central and the southernmost are formed by hypothetical lines (imagery lines) that divide the Gulf of Suez according to a similar pattern to the Gulf of Aqaba (Fig. 1) [3].

According to [1], the chrono-stratigraphy of the Gulf of Suez area is subdivided into three major depositional cycles: prerift (pre-Miocene units), synrift (Miocene units) and postrift (post-Miocene units). The formations which were deposited from a postulated Cambrian to Oligocene time are Nubia (A, B, C and D), Raha, Abu Qada, Wata, Matulla, Brown Limestone, Sudr, Esna, Thebes and Abu Zenima formations. Most of these formations are good to excellent reservoirs, except for the Brown Limestone Formation which acts as the main as well an excellent source rock in the Gulf of Suez [3,5].

The Lower-Middle Miocene formations are Nukhul, Rudies, Kareem and Belayim which form complete petroleum systems characterized by the presences of good source, reservoir and seal rocks. The Upper Miocene formations are South Gharib and Zeit formations which are composed mainly of salts and anhydrites. The post rift deposits are represented by Wardan and Zaafarana formations of Pliocene to Recent age [5] (Fig. 2).

Saqqara Oil Field, which was discovered in 2003 and is still being investigated, is one of the biggest oil fields in the Gulf of Suez. The Saqqara Oil Field is situated 3.5 km west of El Morgan Oil Field, 7.5 km south of Ramadan Oil Field and 3.5 km east of Edfu Oil Field. Saqqaraa Oil field is located between longitudes from 33° to 33°50'E and latitudes from 28° to 28°50'N (Figs. 3,4).

Two of the several drilled wells that are dispersed around the region were chosen to estimate the hydrocarbon potentiality

of the subsurface Matulla sandstone reservoir in the area that is being studied in order to define the petrophysical properties of the sand units.

Extensive studies have conducted to understand the complexity of the Matulla reservoir. [5,23].

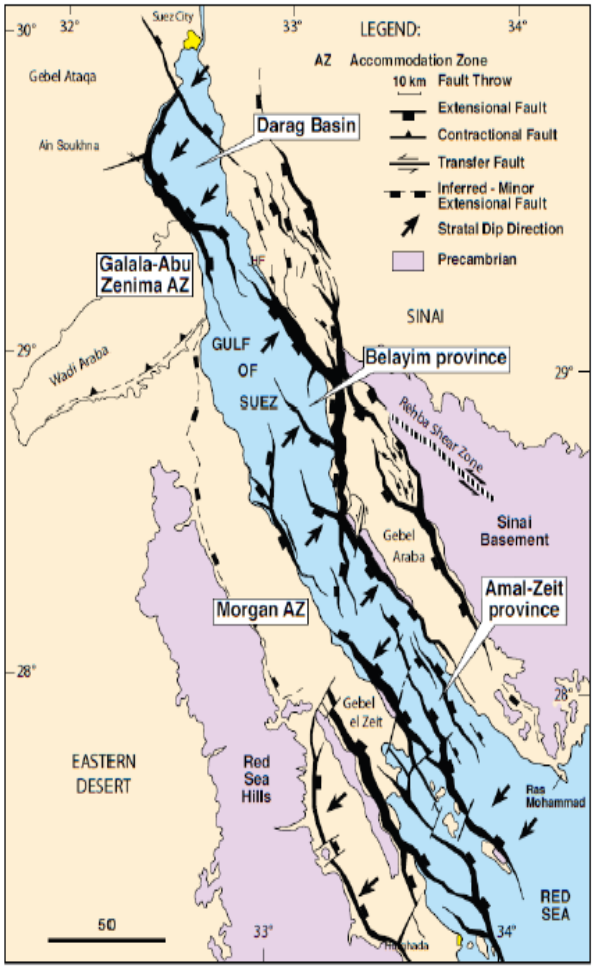

Figure 1: Tectonic and structural provinces in the Gulf of Suez [24].

Reservoir characterization typically determines the gross amount of the trap that may contain hydrocarbons, the precision of reservoir assessment, including thickness, among other factors. Each reservoir's petrophysical characteristics are essential for understanding and estimating parameters from well log data, such as porosity and water saturation [25].

Thus, the goal of this study is to evaluate the reservoirs' hydrocarbon potential by assessing their petrophysical properties utilizing a variety of geology and well logging data from two wells. To facilitate the development of the Saqqara Oil Field.

The possible reservoir zones in the wells under examination were then ascertained by looking through the mud logs. The water saturation (Sw), hydrocarbon saturation (Sh), effective porosity (PHIE) and shale volume (Vsh) in each well were then determined using the wire-line logs and a gamma-ray log. The shale volume and effective porosity were determined using different equations [26]. The water saturation was estimated using the Indonesian model [27]. prospect maps were generated following reservoir analysis to identify promising blocks for reservoir development and to propose well-planning strategies.

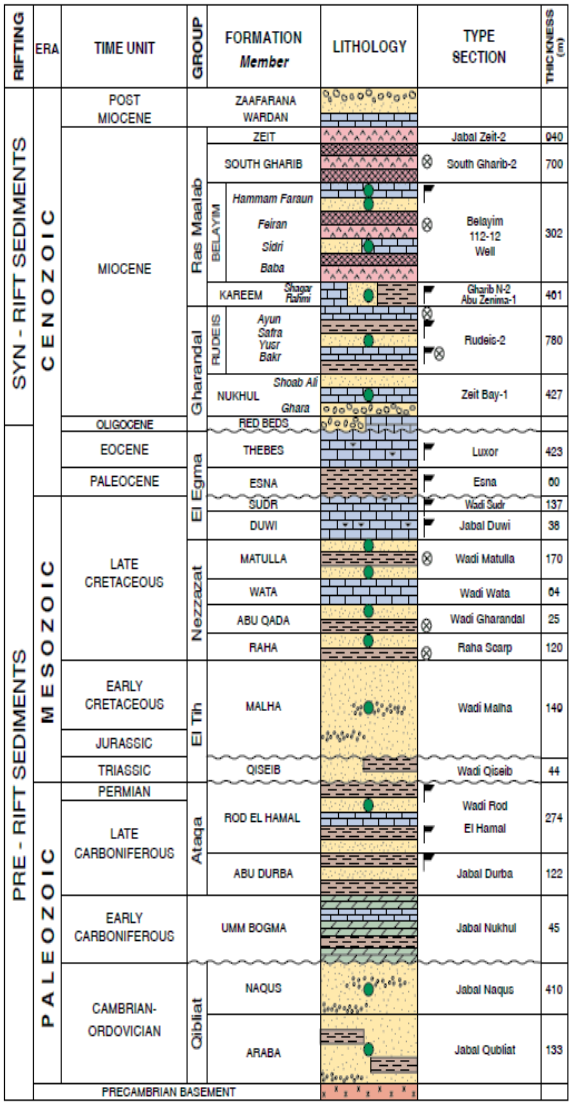

Figure 2: Stratigraphic column of the Gulf of Suez [28].

2. Geologic Setting

The Gulf of Suez originated as the northern extension of the continental rift zone known as the Red Sea, which was active between the Late Oligocene and the end of the Miocene [2]. Even though the Red Sea reached an oceanic stage of sea floor spreading when the Dead Sea Transform expanded east of the Gulf of Suez, the gulf was closed off at a very early stage of rifting [29,32]. Most of the motion that occurs between Africa and Arabia north of the Red Sea is now accommodated by the Dead Sea Transform Plate Boundary [29].

The Gulf of Suez was formed when the water filled the lowest portion of the remaining rift topography during its brief post-rift period. One of the earth's most heavily faulted regions is represented by the gulf (Fig. 5). The rift trends that resulted from the motions of the Nubian, Arabian and Sinai plates the E-W (Tethyan) Trend and the (NNE–SSW) Aqaba Trend have shaped the region's current structure. These fracture systems may still exist today [34].

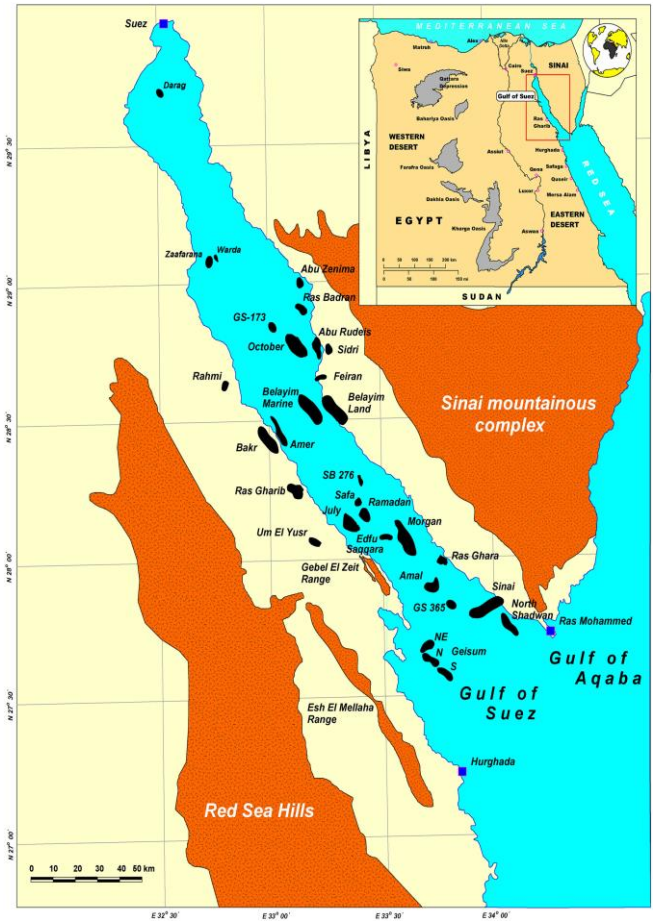

Figure 3: Map represents the location of the area under investigation " Saqqara Oil Fields, south-central Gulf of Suez, Egypt."[33].

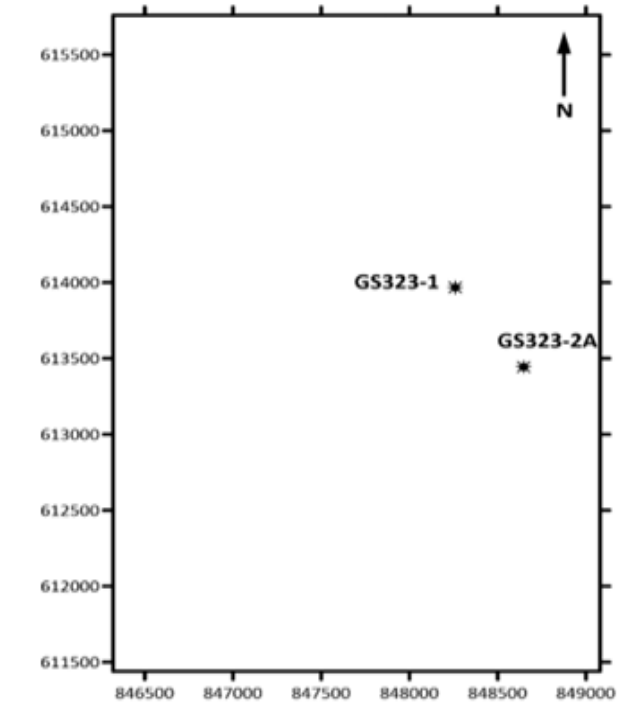

Figure 4: Location base map of Saqqara Field wells.

Crust strain and collapse were brought on by this tensional movement and subsidence. Suction transports possible source rocks to depths where rift basins are conducive to the production of hydrocarbons, whereas stretching movement can cr ɐ hydrocarbon-accumulating petroleum structural traps in the fault blocks. [36].

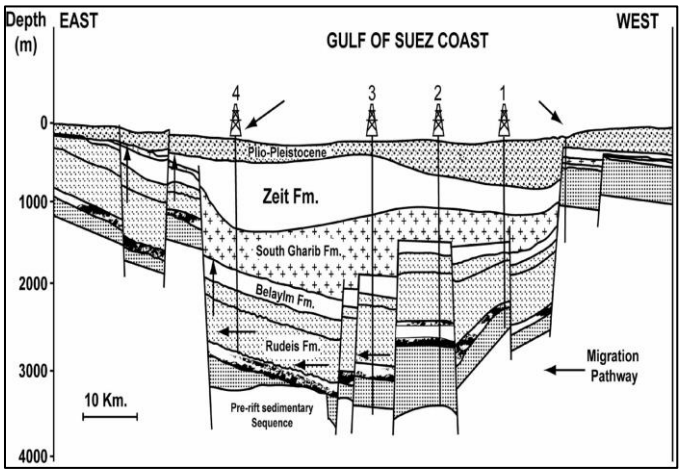

Figure 5: Cross section showing the intensely faulted Gulf of Suez [35].

The age range of the lithostratigraphic units in the Gulf of Suez spans from the Pre-Cambrian to the Holocene. A simplified generalised stratigraphic section of the research region is displayed in (Fig. 2). The Cenozoic rifting may have caused the Gulf of Suez's stratigraphic succession to be divided into three lithostratigraphic mega-sequences: pre-rift, syn-rift and post-rift [37]. These units differ with respect to their hydrocarbon significance, lithology, thickness, areal distribution and depositional environment [1].

The Cambrian to the Eocene was covered by the pre-rift stratigraphic sequence. Pre-rift sediments were deposited on the top of the Pre-Cambrian basement that showed no signs of tectonic movement [38]. At the base, clastic Nubian sandstones were deposited from the Paleozoic to the Lower Cretaceous Albian, which were followed by a phase of marine transgression [39]. A series of carbonate and clastic interbeds were produced as a result of the sea incursion. The following formations, arranged from base to top, comprise the Upper Cretaceous carbonates and clastics sequence: Raha, Abu Qada, Wata, Matulla, Brown Limestone and Suder (Chalk). Paleocene and Eocene shales, carbonates and marls were deposited throughout the Lower Tertiary, indicating that the marine transgression persisted at that time. The final phase of the transgression environment regime, which has ruled since the Cenomanian, was governed by Eocene deposits [39].

Miocene and Oligocene sediments make up the syn-rift stratigraphic series. Continental or extremely shallow sea conditions were typical across the Gulf area throughout the Oligocene [40,41].

This study focuses on the Matulla Formation of the Late Cretaceous period. Its lithology is composed of marls, limestones, shales and several sandstone strata. Its typical thickness ranges from 70 to 500 feet.

Generally speaking, sandy shales that grade into shales towards the top indicate the upper portion of the Matulla

Formation. The Brown Limestone Formation of the Sudr Formation, which sits on top, contains radioactive, dark brown, organic-rich limestones. An abrupt split indicates the beginning of a distinct depositional environment [38].

3. Data and methodology

The datasets used in this study were provided by the Gulf of Suez Petroleum Company (GUPCO) under an agreement with the Egyptian General Petroleum Corporation (EGPC).

It includes the geologic reports, well's location and base maps, core analysis data and wire-line logs for GS323-1 and GS323-2A wells.

The two wells contain open hole logs (resistivity (RES), gamma-ray (GR), calliper (CALI), neutron/density (Neu/Den), and sonic (DT) for the two wells. The available log data were combined to conduct a specific petrophysical evaluation of the reservoir.

Additionally, accessible composite logs help in lithologic description and locating hydrocarbon-bearing zones. Furthermore, core reports have been examined in order to adjust the petrophysical analysis.

An interpretation procedure was carried out to determine the reservoir's characteristics (shale volume, porosity, permeability, water and hydrocarbon saturations and net pay thickness determination). The formation evaluation procedure was carried out using the Techlog software package.

Using the formation assessment technique, the petrophysical properties of the studied reservoir are ascertained from the well-logging data. This system's theory states that well logging data analysis is based on the thorough use of techlog computer software, ready-made charts, cross-plots and equations for the relevant petrophysical parameters, particularly those related to lithology, porosity, water saturation and hydrocarbon saturation.

The well logging analysis process includes measurements for the formation temperature, shale volume (V_{sh}), total porosity (Δt), effective porosity (Φ_{eff}), water resistivity (R_w), water saturation (S_W) and hydrocarbon saturation (S_{hc}).

3.1. Determination of lithology

The lithology and porosity of rocks may be determined using a few standard methods.

- **Neutron-Density Cross-plot**

The neutron-density cross-plot may be used to identify common reservoir rocks including quartz sandstone, calcite (limestone) and dolomite, as well as shale and certain evaporites. It's also useful for identifying gases [42,43].

- **Sonic-Neutron Cross-plot**

When clay concentration is minimal, sonic-neutron can be employed to distinguish between common reservoir rocks. Sonic-neutron is a useful tool for identifying evaporated minerals and distinguishing between shale and a single known reservoir rock [42,43].

- **MID plot**

A cross-plot approach called the Matrix Identification Plot (MID) is used to determine the matrix, lithology and secondary porosity. It needs information from neutron, sonic and density records [42].

Schlumberger charts are a vital technique that yields precise results for lithological identification. To establish an apparent matrix density, the density and neutron logs are merged, (ρ_{maa}) as shown in equation (1) and the neutron and sonic logs are combined to define an apparent matrix travel time, (Δt_{maa}) as shown in equation (2):

$$\rho_{maa} = \frac{\rho_b - (\emptyset_{ND} \times \rho_{fl})}{1 - \emptyset_{ND}} \dots\dots\dots\dots (1)$$

$$\Delta t_{maa} = \frac{\Delta t - (\emptyset_{SD} \times \Delta t_{fl})}{1 - \emptyset_{SN}} \dots\dots\dots\dots (2)$$

where: (ρ_{maa}) is the apparent matrix density in g/cm^3, (Δt_{maa}) is the apparent matrix travel time in μsec/ft, (ρb) is the bulk density from the log, (ρ_{fl}) is the density of the fluid, (Δt) is the interval transit time from the log, (Δt_{fl}) is the interval transit time of the fluid, (Φ_{ND}) is the neutron density cross-plot porosity and (Φ_{SN}) is the sonic neutron cross-plot porosity [42].

Once the apparent matrix density and the apparent matrix travel time have been determined, they are cross plotted on the MID plot [42].

3.2. Shale volume calculation (V_{sh})

Determining the shale volume is one of the most crucial characteristics that sets reservoir rocks apart from non-reservoir rocks [44].

In this study, the presence of feldspars in the Matulla sandstone give higher values of gamma-ray. Therefore, the neutron-density method will be useful in this investigation because the presence of feldspars will affect the V_{sh} calculations made by the linear method and other non-linear methods.

So, the shale volume can be calculated from the following equation (3),

$$V_{sh} = \frac{\Phi n - \Phi d}{\Phi nsh - \Phi dsh} \dots\dots\dots\dots (3)$$

where: (V_{sh}) is the shale volume (%), (Φn) is the neutron log reading in the sand zone, (Φd) is the density log reading in the sand zone, (Φn_{sh}) is the average neutron log reading for shale in that formation and (Φd_{sh}) is the average density log reading for shale in that formation [44].

3.3 Determination of porosity (Φ)

Porosity is known as the volume of void or pore spaces (V_p) divided by the total bulk volume (V) of the rock. Density, neutron and sonic logs are the three commonly used log-derived porosity measurement tools. In this inquiry, the readings from these three techniques will be utilized to establish the average porosity for these reservoirs. Sonic logs are less susceptible to fluctuations in boreholes and mud cake than density and neutron logs.

To account for the impacts of varied lithology in complicated reservoirs, the porosity can be calculated using singles porosity log that measures sonic, density or neutron porosity as well as using a combined of porosity logs [44].

- **Porosity from the sonic log (Φs).**

The porosity can be calculated from the sonic log using equations (4) and (5),

$$\emptyset s = \frac{\Delta t - \Delta t_{ma}}{\Delta t_f - \Delta t_{ma}} \times \frac{1}{C_P} \dots\dots\dots\dots\dots (4)$$

$$C_P = \frac{\Delta t_{sh}}{100} \dots\dots\dots\dots\dots\dots\dots (5)$$

where: (Φs) is the porosity from the sonic log, (Δt) is the transit time from the sonic log, (Δt_f) is the transit time of the formation fluid, which we need to provide, (Δt_{ma}) is the transit time of the matrix, which we need to provide, (Δt_{sh}) is the specific acoustic transit time in adjacent shales and (C_P) is the compaction correction factor [42].

- **Porosity from the density (Φd)**

The porosity can also be estimated from the density log utlizing equation (6),

$$\emptyset d = \frac{\rho_{ma} - \rho_b}{\rho_{ma} - \rho_f} \dots\dots\dots\dots (6)$$

where: (Φd) is the porosity from the density log (%), (ρ_{ma}) is the density of the matrix (gm/cm^3), (ρ_f) is the density of the formation fluid saturating the rock immediately surrounding the borehole, usually mud filtrate, and (ρ_b) is the bulk density (log value) [42].

- **Porosity from the neutron log (Φ_n).**

On the other hand, the prosity can be estimated using neutron log, where the neutron method responds to the presence of hydrogen. So, the neutron log measures liquid-filled porosity in clean formations with water or oil-filled pores. The measured neutron porosity decreases when gas is introduced into pores instead of oil or water; this phenomenon is known as the "gas effect". The measured neutron porosity is lower than the formation porosity, it increases when clays are present in the formation matrix; this phenomenon, known as the "shale effect" that produced by the presence of clays and surpasses the real formation porosity [42].

Consequently, the neutron porosity must be corrected using equation (7),

$$\emptyset_N = \emptyset log - V_{sh} * \emptyset_{nsh} \dots\dots\dots\dots\dots (7)$$

where: (Φ_N) is the porosity from the neutron log (%), (Φlog) is the apparent neutron porosity reading on the log, (Φ_{sh}) is the neutron porosity of shale and (V_{sh}) is the volume of shale [45].

- **Porosity from the neutron-density log (Φ_{ND})**

The formation porosity can be determined by integration of two porosity readings from the density and neutron logs.

The neutron-density porosity can be calculated from equation (8),

$$\emptyset_{ND} = \sqrt{\frac{\emptyset_N{}^2 + \emptyset_D{}^2}{2}} \dots\dots\dots (8)$$

where: (Φ_{ND}) is the neutron density porosity, (Φ_D) is the porosity calculated from the density log at the depth for which the effective porosity is calculated (i.e., zone of interest), and (Φ_N) is neutron porosity at the depth for which the effective porosity is calculated (i.e., zone of interest) [42].

- **The total porosity (Φt)**

After the total porosity has been determined from the various methods, the final total porosity is determined by driving the average readings between the sonic, density and neutron total porosities.

3.4. Estimation of effective porosity (Φ_{eff})

To eliminate the impact of shale content on rock the porosity readings, it is crucial to adjust total porosity for the shale effect by determining the effective porosity.

There are two adjustments that must be made before using the effective porosity calculation. The first one corrects this porosity to quartz sandstone porosity for each type of neutron instrument by utilising the average porosity values from both direct readings of density and neutron logs. In the second one, the volume of the clay is calculated using the neutron-density approach, a non-linear equation [42,45].

Effective porosity ($\emptyset_{eff}$) can be calculated from equation (9):

$$\emptyset_{eff} = \emptyset_t - (V_{sh} * \emptyset_{sh}) \dots\dots\dots (9)$$

where: ($\emptyset_{eff}$) is the effective porosity, ($\emptyset_t$) is the total porosity, (V_{sh}) is the shale volume and ($\emptyset_{sh}$) is the porosity of shale. (Neutron porosity reading in 100% shale or clay) [42,45] .

3.5. Water resistivity estimation (R_W)

Two of the most significant variables influencing and directing the determination of the formation water resistivity (R_w) are salinity and temperature. Low resistivity readings are associated with higher salinity and vice versa. Reduced resistivity results from higher temperatures and vice versa.

The R_w value should be always correlated with the ambient temperature. There are several formulae available for estimating the resistivity of formation water saturation, some of which are as follows [44]:

- **Water resistivity from Archie's equation:**

The connate water resistivity (R_w) is used to calculate the water saturation in the uninvaded zone (S_W) according to the Archie equation (10) [46,47].

$$R_W = S_W{}^2 * \emptyset^2 * R_t \dots\dots\dots\dots (10)$$

where: (R_W) is the water resistivity, (R_t) is the deep resistivity in the uninvaded zone and (Φ) is the porosity.

- **Water resistivity from the Pickett plot**

Plotting resistivity (R_t) on the X-axis versus porosity (Φ) on the Y-axis on a log-log plot (logarithmic scale) produces the Pickett cross-plot, which is the graphical representation of the Archie's equation. The resulting linear equation has the following form (11 and 12):

$$y = mx + b \dots\dots\dots\dots\dots\dots (11)$$

$$\log R_t = \log (a R_w) - m \log \Phi \dots\dots (12)$$

where: ($a*R_w$) represents the intersection of the Rt line with the vertical axis at 100% Φ, and the cementation factor (-m) is the slope of the Rt [48,49].

3.6. Determination of water saturation (S_w)

The fundamental petrophysical parameter used to distinguish a distinct reservoir is the water saturation (S_w) [3]. There are many methods used to calculate the water saturation of the reservoir. Therefore, the methods that are used to calculate the water saturation vary depending on the type of the

rocks that make up the reservoir.

- **The stimation of (S_w) clean reservoirs**

Determination of the water saturation in clean reservoirs use the Archie equations (13 and 14):

$$(Sw)^n = \frac{F \cdot R_W}{R_t} \quad \ldots\ldots\ldots (13)$$

$$\mathbf{F = \frac{a}{\emptyset^m}} \quad \ldots\ldots\ldots\ldots\ldots (\mathbf{14})$$

where: (S_w) is water saturation, (F) is the formation resistivity factor, (a) is the tortuosity factor, (Φ) is the porosity, (R_W) is the resistivity of formation waters, (R_t) is the true formation resistivity, (n) is the saturation exponent, and (m) is the cementation factor. (Usually, n=2, m=2.15 and a=0.62) [46].

- **Eestimation of (Sw) Shaly Sand Reservoirs**

In the case of the presence of shaly sand reservoirs, we use the Indonesia method to estimate the water saturation (15),

$$S_w = \left(\frac{V_{sh}^{\,1-(0.5 * V_{sh})}}{\left(\frac{R_{sh}}{R_t}\right)^{0.5}} + \left(\frac{R_t}{\frac{a * R_w}{m}} \right)^{0.5} \right)^{-2/n} \quad \ldots\ldots\ldots (15)$$

where: (S_w) is the water saturation, (V_{sh}) is the shale volume, (R_w) is the resistivity of formation waters, (R_t) is the true formation resistivity and (R_{sh}) is the resistivity log reading in 100% shale. (Usually, n=2, m=2.15 and a=0.62) [42].

3.7. Determination of permeability (K)

The ease with which liquids may move through a rock body is measured as permeability; while porosity is correlated with permeability, it is not always reliant upon it. Empirical formulae were used to predict the permeability for this investigation. The permeability of the studied reservoirs was calculated using the Wyllie and Rose equation.

Permeability can be estimated in the case of an oil-bearing and gas bearing reservoir using equations 16 and 17 respectively.

$$K = \left(250 \times \frac{\emptyset^3}{S_{W\,irr}} \right)^2 \quad \ldots\ldots\ldots\ldots (16)$$

$$K = \left(79 \times \frac{\emptyset^3}{S_{W\,irr}} \right)^2 \quad \ldots\ldots\ldots\ldots (17)$$

where: (K) is the permeability (millidarcy), (Φ) is the porosity and ($S_{w\,irr}$) is the irreducible water saturation [3,44].

3.8. Estimation of hydrocarbon saturation (S_{hc})

The hydrocarbon saturation can be estimated by the relationship between it and the water saturation as shown in equation (18),

$$S_{hc} = 1 - S_W \quad \ldots\ldots\ldots\ldots (18)$$

where; (S_{hc}) is the hydrocarbon saturation and (S_w) is the water saturation [50].

3.9. Net pay thickness determination

The Net-pay thickness is computed by averaging the pay net flag using the Techlog software.

3.10. Net -to- Gross ratio

The term "net pay" describes the thickness of an interval-permeable porous zone that contains a marketable amount of hydrocarbon. The ratio of the thickness of the net pay to the thickness of the total compensation is expressed as net to gross ratio. In the volumetric computation of reservoirs, this ratio is crucial. Three crucial parameters are needed to calculate the net pay. These numbers correspond to permeability to reservoir fluids, water saturation and porosity.

4. Results and Discussion

(Figs. 6,7), respectively, show the petrophysical data logs of the two wells (GS323-1 and GS323-2A) that were chosen from the Saqqara oilfield.

4.1. Lithology determination

Inspection of different types of well logging results in two selected wells revealed that the lithology of Matulla reservoir is not uniform throughout the formation, but is composed mainly of mixed lithology as carbonates, sandstones and shales. The lithology of Matulla reservoir was identified using different techniques as follows:

- **Density-Neutron Cross-plot**

(Figs. 8,9) represent density-neutron cross-plots of the two selected wells (GS323-1 and GS323-2A) for the Matulla formation. Examining (Fig. 8), it was found that the GS323-1 well predominantly consists mainly of three rock facies: carbonates, shales and sandstones. Conversely, (Fig. 9) shows that the GS323-2A well contains carbonates and shales only but lacks sandstones, suggesting that the sandstone is disappearing towards the southeast.

- **Neutron-sonic cross-plot**

(Figs. 10,11) represent the neutron-sonic cross-plots of the two selected wells of the Matulla Formation which show the same results of the previous method of lithology determination.

(Fig. 10) represents the Matulla reservoir lithology in the GS323-1 well, and it shows that the formation lithology is made up mainly of sandstone, shale and carbonate rocks confirming the same results of the former technique. On the contrary, (Fig. 11) exhibits the lithology of the Matulla reservoir in the GS323-2A well, and it shows that the formation lithology is made up mainly of carbonate rocks and also a few percentages of shales content with absence of sandstone.

- **MID Plot**

(Figs. 12,13) represent the MID plots of the two selected wells of the Matulla Formation which show the same results as the two previous methods where the three-formation lithology (carbonate, shales, and sandstones) are present in the GS323-1 well and only carbonates and shales contents are present in the GS323-2A well.

4.2. Estimation of shale volume (V_{sh})

The shale volume was calculated using the neutron-density method because the gamma-ray method gives a high value in the Matulla sandstone reservoir as a result of the presence of feldspars. The shale volume scale is from zero to 100% percent and the shale volume symbol is (V_{sh}).

The results of this method indicated that the Matulla reservoir has range value of shale volume between 0% and 100% in some feets in both of the two wells and an average value of 1.9% and 3.1% in the GS323-1 and GS323-2A wells respectively, which indicates that the Matulla Formation is a good reservoir (Figs. **6,7**).

4.3. Estimation of total porosity (Φt)

The total porosity was determined from sonic, density and neutron logs in the selected two wells. The final total porosity (PHIT_final) scale is from zero to 30% percent and the final total porosity symbol is After the determination of total porosity from the different porosity logs, the average reading between sonic, density and neutron total porosity is driven and called the final total porosity. The results showed that the average porosity values are 14% and 13%, with minimum value of 0.7% and 1.4 % and with maximum value of 24% and 16.1% in the GS323-1 and GS323-2A wells respectively (Figs. **6,7**).

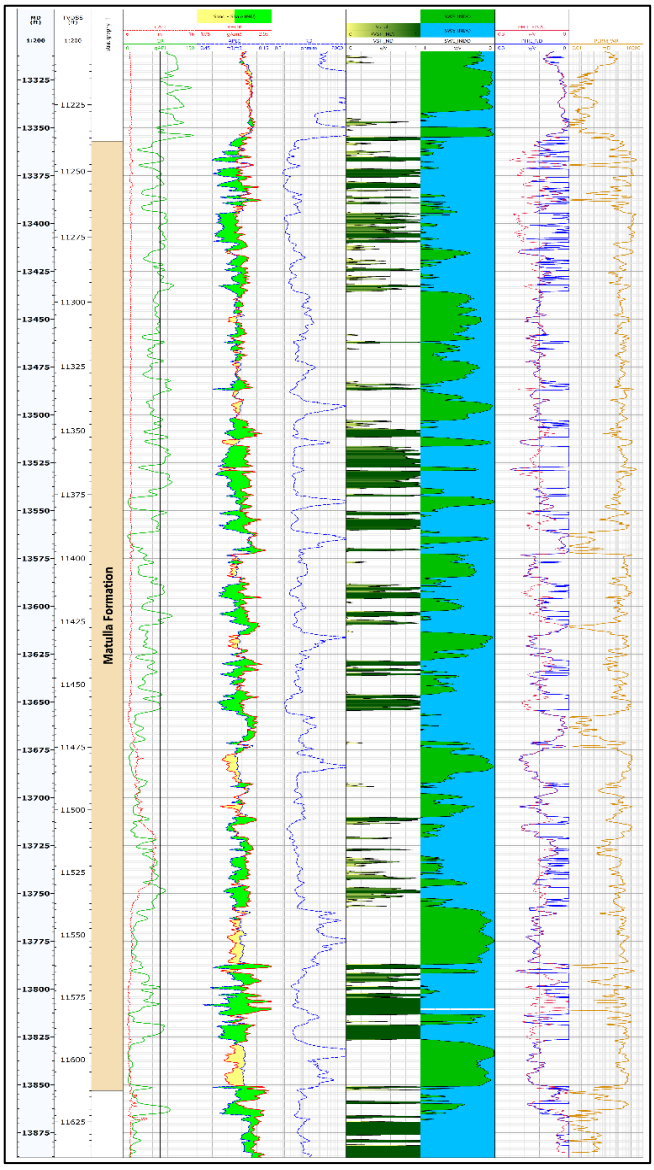

Figure 6: well logging with assessment for Matulla reservoir in examined well GS323-1.

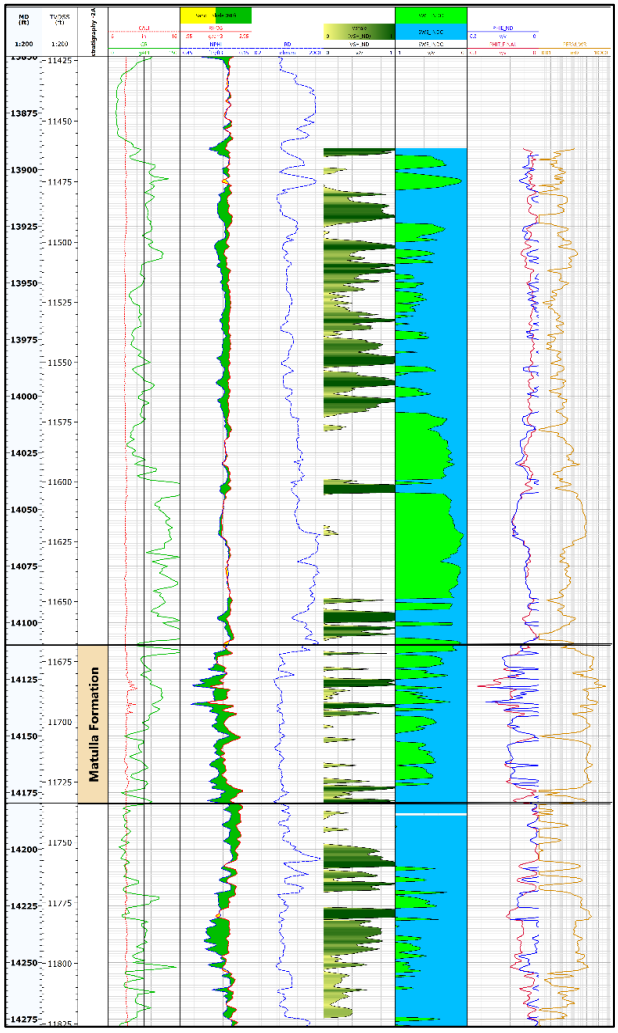

Figure 7: well logging with assessment for Matulla reservoir in examined well GS323-2A.

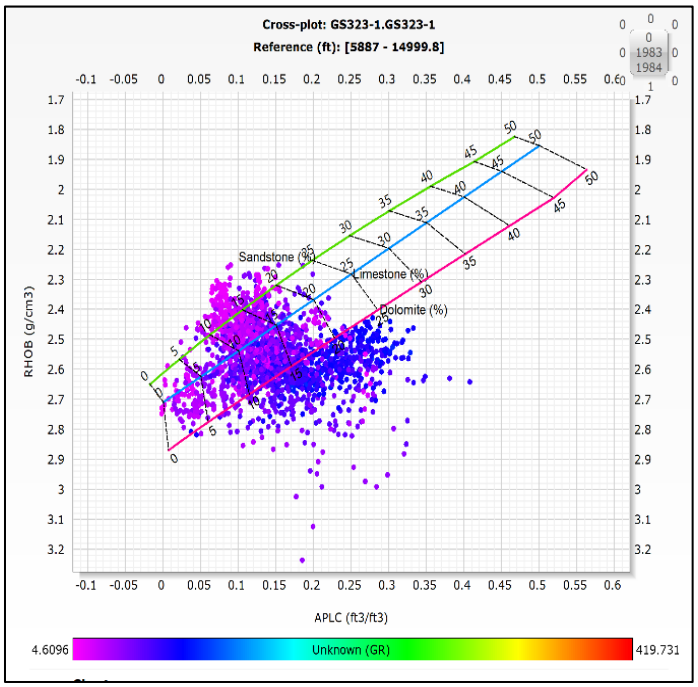

Figure 8: Neutron-density cross-plot for the GS323-1 well.

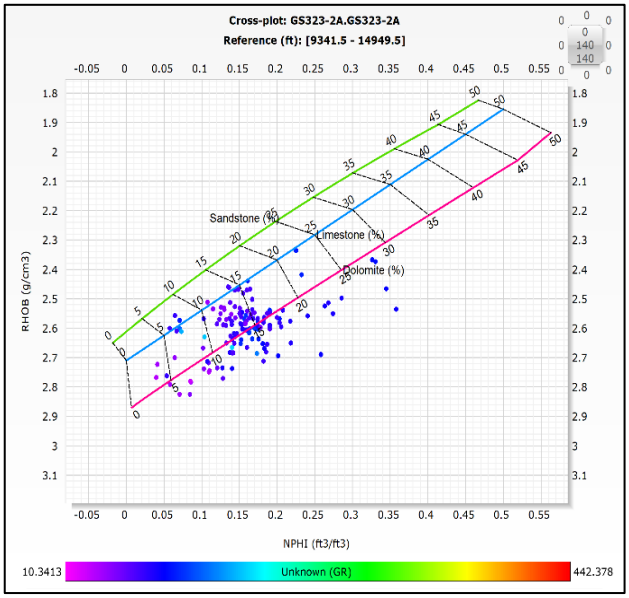

Figure 9: Neutron-density cross-plot for the GS323-2A well.

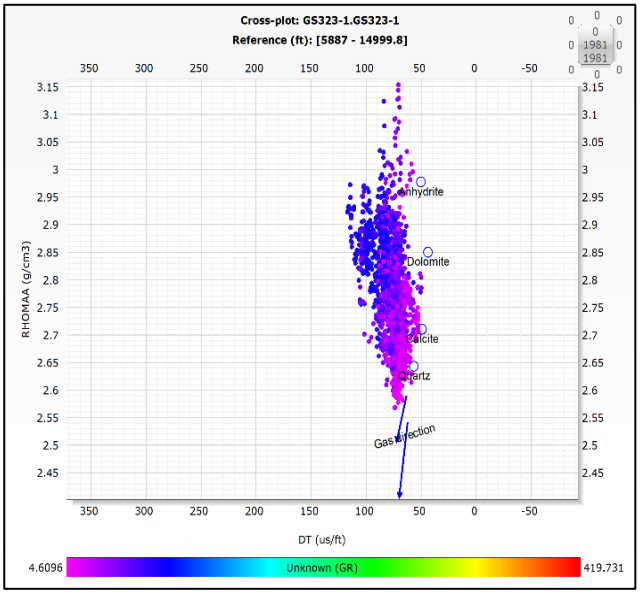

Figure 12: MID plot of the Matulla reservoir for the GS323-1 well.

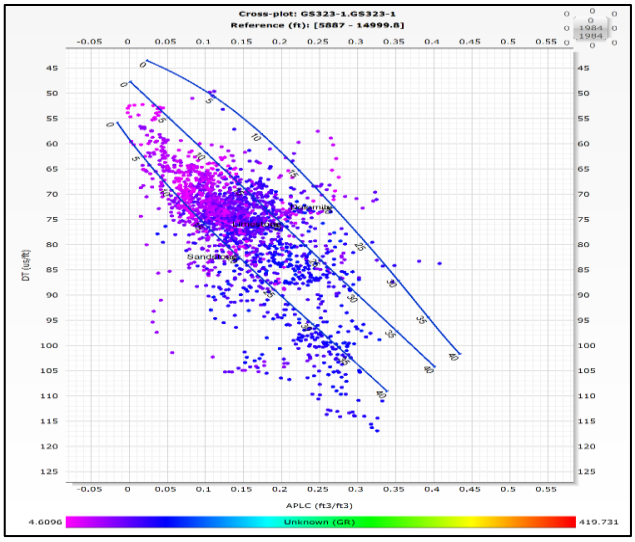

Figure 10: Neutron-sonic cross-plot of the Matulla reservoir for the GS323-1 well.

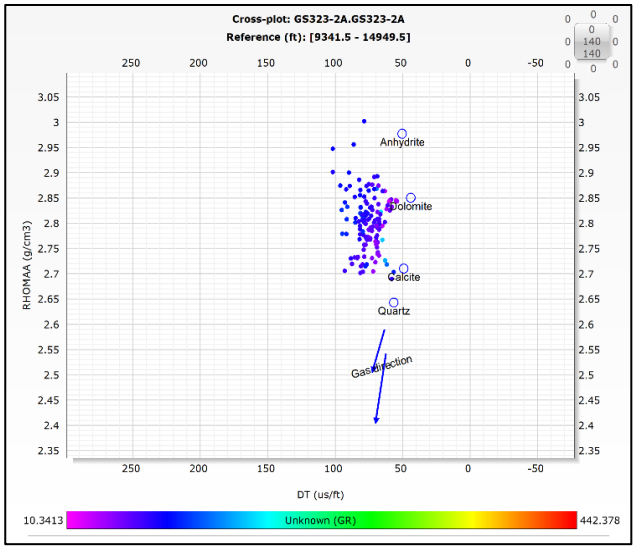

Figure 13: MID plot of the Matulla reservoir for the GS323-2A well.

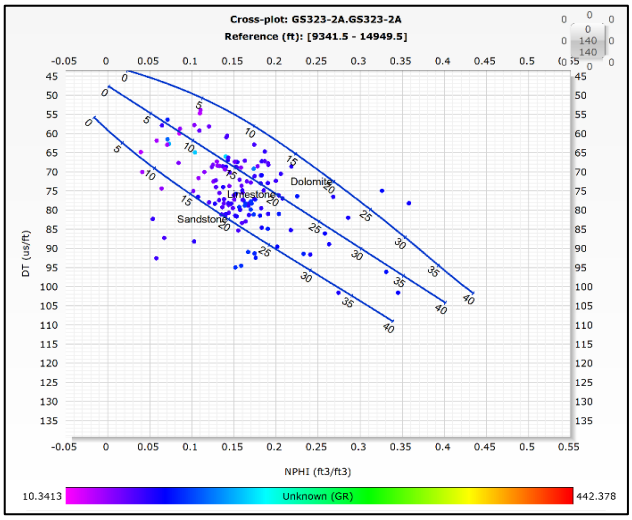

Figure 11: Neutron-sonic cross-plot of the Matulla reservoir for the GS323-2A well.

4.4. Estimation of effective porosity (Φ_{eff})

Based on the application of this method to the Matulla reservoir wells, the effective porosity ($Ø_{eff}$) analysis of the Matulla sandstone unit in the GS323-1 and the GS323-2A wells show that the average effective porosity values in the two wells are good with values equal 13.7% and 12.5%, minimum value of 0.2% and 0% and with maximum value of 20% and 22% in the GS323-1 and GS323-2A wells respectively, these results reflect that the reservoir rock's varied pore space which enhance the ability of the rock to store hydrocarbons. This result is matched good with the result of [19]. The effective porosity scale is from zero to 30% percent and the effective porosity symbol is (PHIE) (Figs. 6,7).

4.5. Water saturation (S_w) determination

- **Water saturation (S_w) determination using the Indonesian method**

The presence of shale in the Matulla reservoir leaded to

calculate the water saturation by the Indonesia method. The water saturation scale is from zero to 100% percent and the water saturation symbol is (S_w) or (SW_INDO).

Based on the application of this method to the Matulla reservoir wells, the water saturation (S_w) analysis of Matulla sandstone in GS323-1 well shows an average water saturation of 32% and in GS323-2A well shows an average water saturation of 46% (Figs. 6,7).

- **Water saturation (S_w) determination from the Pickett plot**

Points representing the Matulla zone in the studied wells are placed above the S_w=50% line in the two selected wells (14 and 15), reflecting the good hydrocarbon potentiality of this reservoir and confirming the completed petrophysical calculations.

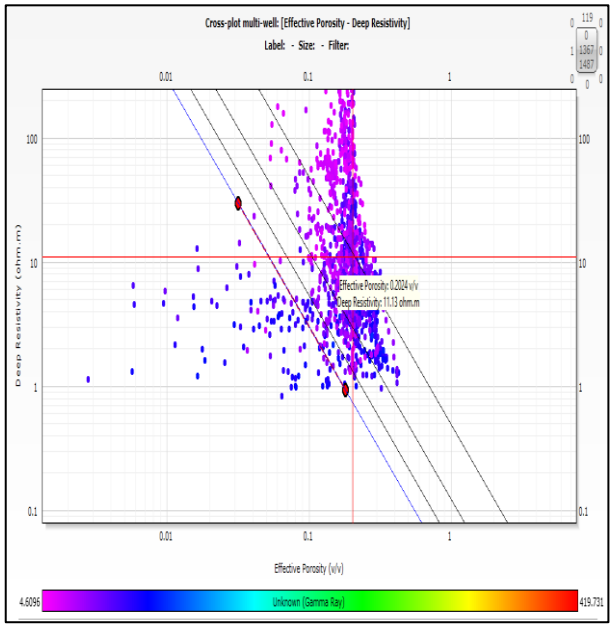

Figure 14: Pickett plot of GS323-1.

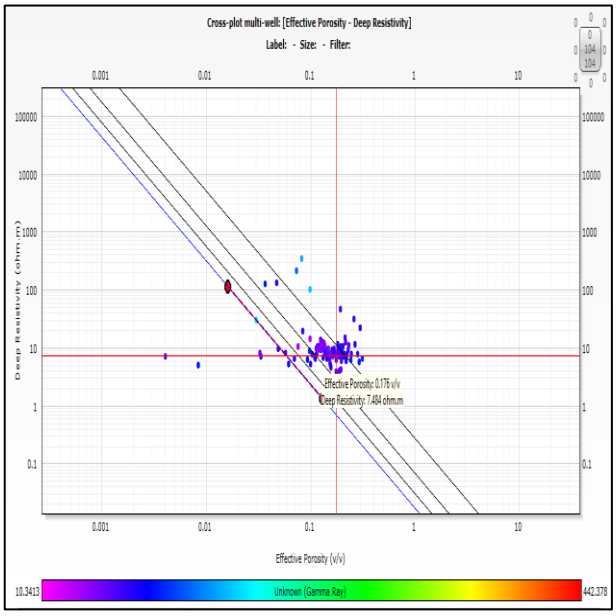

Figure 15: Pickett plot of GS323-2A.

4.6. The determination of permeability (K)

The application of the Wyllie and Rose equation to the Matulla sandstone reservoir wells, permeability scale is logarithmic and starts from zero to 10000 mD and the permeability symbol is (K) or (PERM_WR).

The average permeability (K) values of the Matulla reservoir in GS323-1 well is 320.71 mD with a minimum value reaching 0.01 mD and maximum value reaching 2962.9 mD, while in GS323-2A well the average permeability (K) reaches 219.37 mD, with a minimum value reaching 0.01 mD and maximum value reaching 3953.66 mD. The wide range of permeability indicates the reservoir heterogeneity, which may affect the fluid flow efficiency within the formation (Figs. 6,7).

4.7. Estimation of hydrocarbon saturation (S_{hc})

Based on equation (18), the hydrocarbon saturation of the Matulla reservoir have average values of about 68% and 54% in GS323-1 and GS323-2A wells respectively.

4.8. Fluid type (Quick look method)

High resistivity values in the Matulla reservoir indicate hydrocarbon zone, so, the application of this method on the Matulla Formation found that the GS323-1 well shows inferred crossover between density and neutron curves (Fig. 6) which indicate oil bearing formation, this result was also concluded from the MID plot (Fig. 12) where the points are not collected on the gas trend, so, it indicates as an oil-bearing formation. From MID plot (Fig. 13) the hydrocarbon type in the GS323-2A well is oil.

4.9. Net pay thickness determination

The net pay thickness was calculated for the Matulla reservoir in the two selected wells. It shows an average value of 150.95.3 ft in GS323-1 well and 24.5 ft in GS323-2A well. The net to gross ratio is about 37% to 40% in the two wells.

Table (1) provides an overview of the average values of the many calculated petrophysical parameters of the Saqqara oilfield's studied wells.

5. Cut-off determination

The lowest or maximum values of specific petrophysical parameters that define reservoir zones are known as petrophysical cutoffs. Petrophysical cutoffs change based on the kind of reservoir, fluid properties and geological environment. Well logs, statistical techniques or core analysis can all be used to ascertain them. Shale volume, porosity and water saturation are the three criteria that are utilised to determine reservoir zones. The net pay of the Matulla reservoir is depicted by these cut-offs in the GS323-2A and GS323-1 wells in (Figs. 16,17) respectively. The workflow table flags for these parameters are displayed in Table (2). The yellow colour represents the rock flag. The green colour represents the reservoir flag, where the shale content and porosity are cut-offs. The red colour denotes the net pay flag, where the three parameters (shale content, porosity, and water saturation) are cut-offs.

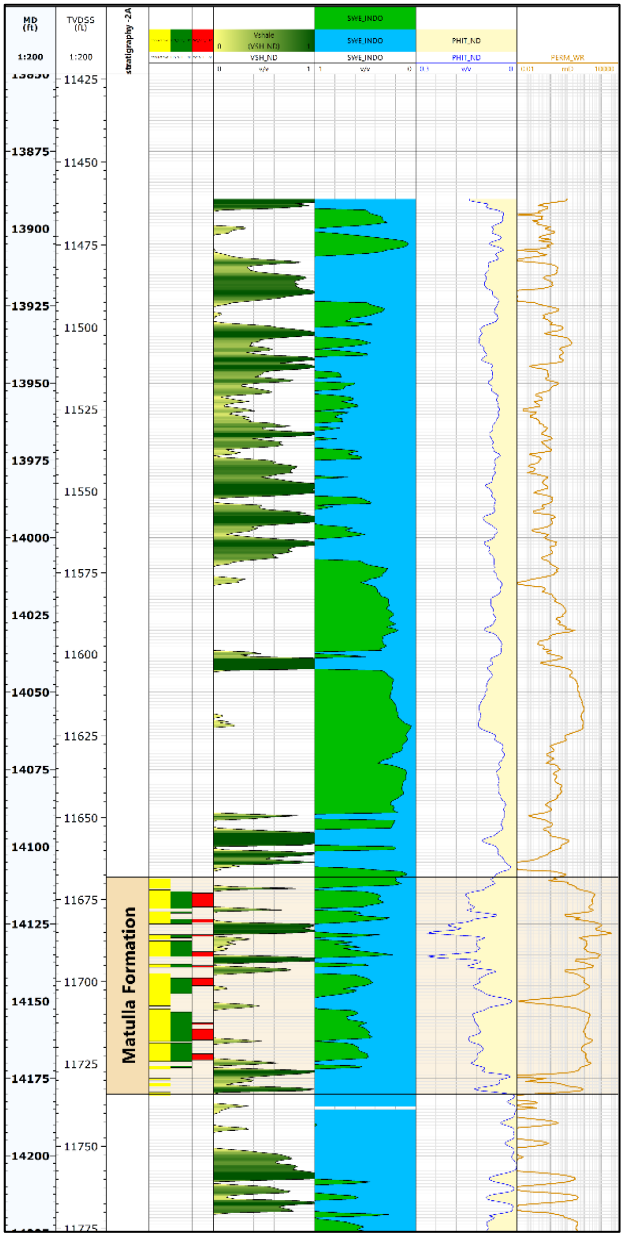

Figure 16: Cut-off of Matulla reservoir in GS323-1 well.

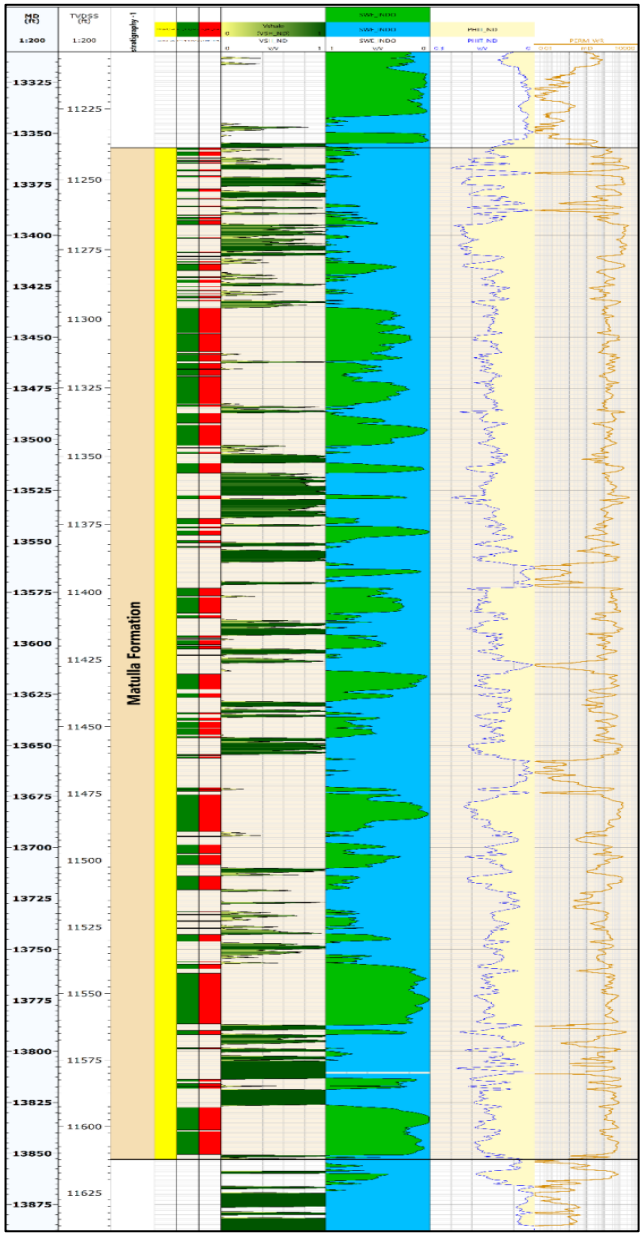

Figure17: Cut-off of Matulla reservoir in GS323-2A well

Table 1: Summary of derived petrophysical parameter of the Matulla reservoir.

Well name	Coordinates	Formation	Depth to the top (ft) TVDSS	Depth to the top (ft) TVDSS	Gross thickness(ft)	Reservoir parameters					
						Net pay thickness (ft)	Net to gross ratio	Shale volume	Effective porosity	Water saturation	Hydrocarbon saturation
GS323-1	X=846850 Y=613050	Matulla	11333.95	11707.71	373.7	150.9	0.4	0.019	0.137	0.32	0.68
GS323-2A	X=846846.84 Y=613046.28	Matulla	11668.3	11734.1	65.84	24.5	0.37	0.031	0.125	0.46	0.54

6. Summary and conclusion

Saqqara oilfield is the studied area which locates in the south-central Gulf of Suez in Egypt. The goal of this study is to evaluate the Upper Cretaceous Matulla reservoir through an analysis of its petrophysical characteristics using several well logging data. The petrophysical properties of the Matulla Formation (effective porosities, shale volume, water and hydrocarbon saturations) were determined using Techlog Program. The average net pay thickness of the

reservoir is 90 feet which were calculated using standard cut-off, where the average percentages of porosity, shale volume, and water saturation were 13.1%, 2.55 and 40%, respectively. According to the previous petrophysical results of the Matulla reservoir, the authors concluded that it is a good reservoir quality with appropriate hydrocarbon potentiality.

Table 2: Workflow table flags of the field cut-offs.

	Flag Name	Flag shading colour	Shale Volume cutoff	Porosity cutoff	Water Saturation cutoff
1	ROCK		yes	No	No
2	RES		yes	Yes	No
3	PAY		yes	Yes	Yes

7. Acknowledgments

The authors would like to thank the Egyptian General Petroleum Corporation (EGPC) and Gulf of Suez Petroleum Company (GUPCO) for providing the dataset and permission to publish this work.

8. Abbreviations

$S_{W:}$	Water saturation
S_h:	Hydrocarbon saturation
Swirr:	Irreducible water saturation
R_t:	Deep resistivity in the un-invaded zone.
Ro:	The resistivity of rock filled with water
RD:	Deep resistivity
R_W:	Water resistivity
RES:	Resistivity
$S_{W:}$	Water saturation
S_h:	Hydrocarbon saturation
Swirr:	Irreducible water saturation
C_P:	The compaction correction factor.
PHIE or Φ_{eff}:	Effective porosity
PHIT or Φ_t:	Total porosity
Φ:	Porosity
Φn:	Neutron porosity
Φnsh:	Neutron porosity of shale
Φnd:	Neutron -density porosity
Φd:	density porosity
Φdsh:	density porosity of shale
Φsn:	Neutron -sonic porosity
Neu:	Neutron
Den:	Dnsity
V_{sh}:	Shale volume
GR:	Gamma ray
Cali:	Calliper
K:	Permeability
ρ_b:	The bulk density.
ρ_{fl}:	The density of the fluid.
ρ_{maa}:	The Apparent matrix density
ρ_{ma}:	The matrix density
Dt or Δt:	The sonic transit time.
Δt_{fl}:	The fluid interval transit time.
Δt_{maa}:	The apparent matrix transit time.
Δt_{sh}:	The transit time in shale.
F:	The formation resistivity factor.
a:	The tortuosity factor.
m:	The cementation factor.
n:	The saturation factor.

CRediT authorship contribution statement:

Conceptualization, Abudeif, A.M. and Tawfik, F.A.; methodology, Tawfik, F.A. and Radwan, A.E.; software, Tawfik, F.A.; validation, Mohammed, A.M. Abudeif, A.M. and Tawfik, F.A.; formal analysis, Tawfik, F.A.; investigation, Abudeif, A.M.; resources, Radwan, A.E. and Tawfik, F.A.; data curation, Mohammed, A.M.; writing—original draft preparation, Tawfik, F.A.; writing—review and editing, Abudeif, A.M.; visualization, Tawfik, F.A.; supervision, Abudeif, A.M., Rawan, A.E., and Mohammed, A. M.; project administration, Abudeif, M.A.; No funding acquisition. All authors have read and agreed to the published version of the manuscript.

Data availability statement

The data used to support the findings of this study are available from the corresponding author upon request.

Declaration of competing interest

The authors declare that they have no known competing financial interests or personal relationships that could have appeared to influence the work reported in this paper.

References

[1] Alsharhan, A., *AAPG bulletin*, 87(1) (2003) 143-180.
[2] Khalil, S. and K. McClay, G*eological Society, London, Special Publications*, 187 (2001) 453-473.
[3] Schlumberger, *"Well evaluation conference."Egypt*, (1984).
[4] Garfunkel, Z., *Geological Survey of Israel Bulletin*, 71 (1977) 1-44.
[5] El-Gendy, N., M. Barakat, and H. Abdallah, *Egypt. Journal of African Earth Sciences*, 129 (2017) 596-609.
[6] Abd El Gawad, E., et al., *Int J Innov Sci Eng Technol*, 3(12) (2016) 74-83.
[7] Abd El Gawad, E., M.S. Hammed, and H.A. El Naggar, SUBSURFACE STRUCTURAL IMAGING AND ARCHITECTURE OF PRE-RIFT SEDIMENTS OF WEST HURGHADA DISTRICT, EGYPT, 2016.
[8] El Sharawy, M.S. and B.S. Nabawy, *Natural Resources Research*, 28 (2019) 1587-1608.
[9] Ewida, H.F. and M.A. Sarhan, *Euro-Mediterranean Journal for Environmental Integration*, 8(3) (2023) 645-664.
[10] Farouk, S., et al., *Geomechanics and Geophysics for Geo-Energy and Geo-Resources*, 9(1) (2023) 36.
[11] Farouk, S., et al., *Geomechanics and Geophysics for Geo-Energy and Geo-Resources*, 8(5) (2022) 130.
[12] Moustafa, A.R. and S.M. Khalil, *The geology of Egypt*, (2020) 295-342.
[13] Sarhan, M.A. and A.M. Basal, *Euro-Mediterranean Journal for Environmental Integration*, 8(3) (2023) 613-623.

[14] Shehata, A.A., et al., *Marine and Petroleum Geology*, 131 (2021) 105160.
[15] Shehata, A.A., et al., *Journal of African Earth Sciences*, 200 (2023) 104890.
[16] Temraz, M. and H. Dypvik, *Journal of Petroleum Exploration and Production Technology*, 8 (2018) 85-98.
[17] Salman, A.M., *Arabian Journal of Geosciences*, 14(12) (2021) 1133.
[18] Salman, A.M., *Carbonates and Evaporites*, 38(4) (2023) 71.
[19] Selim, E.S. and M.A. Sarhan, *Marine Geophysical Research*, 45(1) (2024) 8.
[20] Ali, A.M., et al., *Natural Resources Research*, 31(1) (2022) 385-413.
[21] Zalat, A., et al., *Australian Journal of Basic and Applied Sciences*, 6(12) (2012) 511-529.
[22] Obaidalla, N.A., et al., *Assiut University Journal of Geology*, 47(2) (2018) 23-40.
[23] Shalaby, M.R. and M.A. Islam, *Journal of Petroleum Exploration and Production Technology*, 7 (2017) 977-989.
[24] Khalil, S.M., *Ph.D. Thesis, Royal Holloway, University of London, London, United Kingdom*, (1998) 1-349.
[25] Horsfall, O., D. Davies, and O. Davies, *International Journal of Applied and Natural Sciences (IJANS)*, 4(5) (2015) 55-64.
[26] Asquith, G.B. and C.R. Gibson, Basic relationships of well log interpretation: chapter I, 1982.
[27] Poupon, A. and J. Leveaux, *in SPWLA Annual Logging Symposium. SPWLA*, (1971).
[28] Alsharhan, A. and M. Salah, *Bulletin of Canadian Petroleum Geology*, 42(3) (1994) 312-331.
[29] Feinstein, S., et al., *Tectonophysics*, 266(1-4) (1996) 203-220.
[30] Garfunkel, Z., I. Zak, and R. Freund, *Tectonophysics*, 80(1-4) (1981) 1-26.
[31] Steckler, M.S. and U.S. ten Brink, *Earth and Planetary Science Letters*, 79(1-2) (1986) 120-132.
[32] Tamsett, D., *Tectonophysics*, 104(1-2) (1984) 35-46.
[33] Corporation, E.G.P., *The Egyptian General Petroleum Corporation New Maadi, Cairo*, (1996).
[34] Dahy, S.A., *Res J Earth Sci*, 2(1) (2010) 08-13.
[35] Younes, M., *Journal of Petroleum Geology*, 26(2) (2003) 211-224.
[36] Lashin, A. and S. Mogren, *Int J Phys Sci*, 7(35) (2012) 5353-5366.
[37] Plaziat, J.-C., et al., *Springer*, (1998) 211-222.
[38] Schutz, K.I., Structure and Stratigraphy of the Gulf of Suez, Egypt: Chapter 2: Part I. Type Basin: Gulf of Suez, 1994.
[39] Omran, M.A. and M.S. El Sharawy, *Arabian Journal of Geosciences*, 7 (2014) 87-107.
[40] Said, R., The Geology of Egypt: Elsevier book company, Amsterdam, 1962.
[41] Tromp, S., *Geological Magazine*, 87(6) (1950) 385-392.
[42] Asquith, G.B., D. Krygowski, and C.R. Gibson, *American Association of Petroleum Geologists Tulsa*, 16 (2004).
[43] Limited, S., *Schlumberger*, (1985).
[44] Radwan, A., *M. Sc. Thesis*, (2014).
[45] Dewan, J., Essentials of modern open-hole log interpretation, 1983.
[46] Archie, G.E., *Transactions of the AIME*, 146(01) (1942) 54-62.
[47] Sarhan, M.A., *Journal of African Earth Sciences*, 158 (2019) 103544.
[48] Pickett, G., *The Log Analyst*, 14(04) (1973).
[49] Pickett-Heaps, J. and D. Northcote, *Journal of Cell Science*, 1(1) (1966) 109-120.
[50] Kumar, M., Basic Well Logging, 1st Edition, CreateSpace Independent Publishing Platform 2017.